Since January 2020 Elsevier has created a COVID-19 resource centre with free information in English and Mandarin on the novel coronavirus COVID-19. The COVID-19 resource centre is hosted on Elsevier Connect, the company's public news and information website.

Elsevier hereby grants permission to make all its COVID-19-related research that is available on the COVID-19 resource centre - including this research content - immediately available in PubMed Central and other publicly funded repositories, such as the WHO COVID database with rights for unrestricted research re-use and analyses in any form or by any means with acknowledgement of the original source. These permissions are granted for free by Elsevier for as long as the COVID-19 resource centre remains active.

Article

Cell Host & Microbe

SARS-CoV-Encoded Small RNAs Contribute to Infection-Associated Lung Pathology

Graphical Abstract

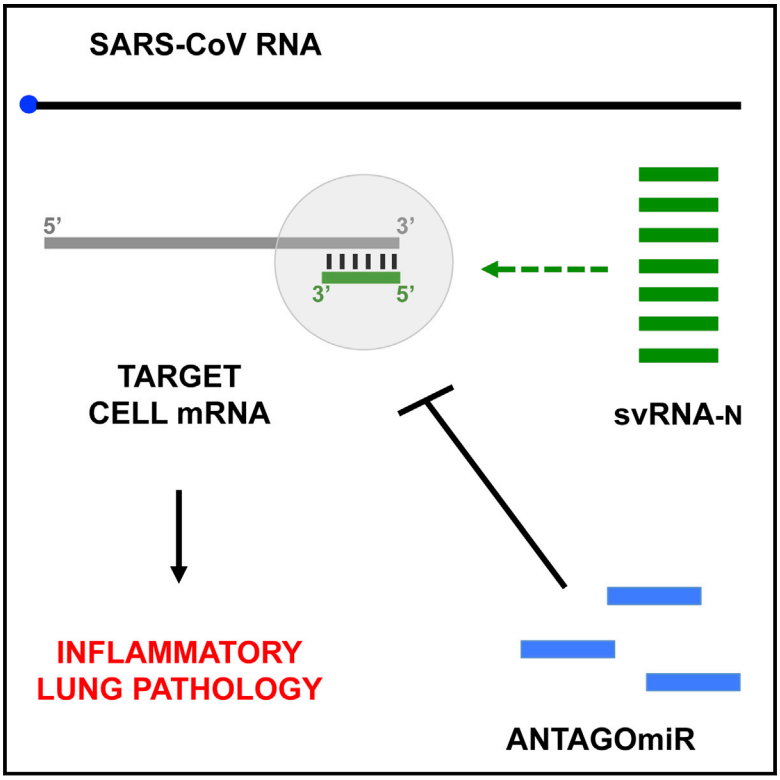

Highlights

- SARS-CoV small viral RNAs (svRNA) were identified in infected lungs and cell culture
- SARS-CoV svRNAs biogenesis was RNase III, cell type, and species independent
- svRNA-N repressed the expression of mRNAs with 3′ UTR specific target sequences
- svRNA-N inhibition in vivo reduced lung pathology and proinflammatory cytokines

Authors

Lucía Morales, Juan Carlos Oliveros, Raúl Fernandez-Delgado, Benjamin Robert tenOever, Luis Enjuanes, Isabel Sola

Correspondence

l.enjuanes@cnb.csic.es

In Brief

SARS-CoV causes exacerbated inflammatory responses, extensive lung pathology, and lethal disease in humans. Morales et al. identify SARS-CoV-encoded small viral RNAs (svRNAs) expressed during lung infection. Virus N gene-derived svRNA (svRNA-N) contributes to enhanced lung inflammatory pathology. Antisense svRNA-N inhibitors significantly reduced pulmonary inflammation during in vivo infection in mice.

Accession Numbers

GSE90624

Morales et al., 2017, Cell Host & Microbe *21*, 344–355
March 8, 2017 © 2017 Elsevier Inc.
http://dx.doi.org/10.1016/j.chom.2017.01.015

CellPress

Cell Host & Microbe
Article

SARS-CoV-Encoded Small RNAs Contribute to Infection-Associated Lung Pathology

Lucía Morales,[1] Juan Carlos Oliveros,[2] Raúl Fernandez-Delgado,[1] Benjamin Robert tenOever,[3] Luis Enjuanes,[1,4,*] and Isabel Sola[1]

[1]Department of Molecular and Cell Biology
[2]Computational Genomics Service
National Center of Biotechnology (CNB-CSIC), Madrid, 28049, Spain
[3]Department of Microbiology, Icahn School of Medicine at Mount Sinai, New York, NY 10029, USA
[4]Lead Contact
*Correspondence: l.enjuanes@cnb.csic.es
http://dx.doi.org/10.1016/j.chom.2017.01.015

SUMMARY

Severe acute respiratory syndrome coronavirus (SARS-CoV) causes lethal disease in humans, which is characterized by exacerbated inflammatory response and extensive lung pathology. To address the relevance of small non-coding RNAs in SARS-CoV pathology, we deep sequenced RNAs from the lungs of infected mice and discovered three 18–22 nt small viral RNAs (svRNAs). The three svRNAs were derived from the nsp3 (svRNA-nsp3.1 and -nsp3.2) and N (svRNA-N) genomic regions of SARS-CoV. Biogenesis of CoV svRNAs was RNase III, cell type, and host species independent, but it was dependent on the extent of viral replication. Antagomir-mediated inhibition of svRNA-N significantly reduced in vivo lung pathology and pro-inflammatory cytokine expression. Taken together, these data indicate that svRNAs contribute to SARS-CoV pathogenesis and highlight the potential of svRNA-N antagomirs as antivirals.

INTRODUCTION

Severe acute respiratory syndrome coronavirus (SARS-CoV) emerged in China in 2002 and spread to more than 30 countries, infecting around 8,000 people and causing 10% mortality in young people and up to 50% in the elderly (Perlman and Netland, 2009). Bats have been identified as zoonotic primary reservoirs for SARS-CoV-associated coronaviruses (CoVs) (Perlman and Netland, 2009), transmitting the virus to humans either directly or through intermediate hosts. The global distribution of bats increases the probability of future emergence of pathogenic human CoVs. To date, there are no vaccines or antivirals approved for either SARS-CoV or other emergent CoVs, such as Middle East respiratory syndrome CoV (MERS-CoV). Understanding the molecular mechanisms of viral pathogenesis will aid in the search for effective and safe therapeutic strategies against known human CoVs and new emergent strains.

SARS-CoV encodes a small transmembrane envelope (E) protein that participates in viral morphogenesis and contributes to the exacerbated inflammatory response associated with acute respiratory distress syndrome (ARDS). An engineered mutant lacking the E protein (SARS-CoV-ΔE) was attenuated in vivo, causing diminished inflammatory pathology in the lung and increased survival (DeDiego et al., 2007). Therefore, the E protein is a virulence factor contributing to SARS-CoV pathogenesis through different mechanisms of action, including NF-kB activation (DeDiego et al., 2014), inflammasome activation through its ion channel activity (Nieto-Torres et al., 2014), and p38 mitogen-activated protein kinase (MAPK) activation through its PDZ-binding motif, which interacts with the cellular protein Syntenin and induces expression of pro-inflammatory cytokines (Jimenez-Guardeño et al., 2014).

In addition to protein components, viral genomes can also encode non-coding RNAs (ncRNAs) differing in size, biogenesis, and function, which are not necessarily comparable to those produced by host cells (Tycowski et al., 2015). It is widely accepted that DNA viruses (Cullen, 2011) and RNA viruses with a nuclear stage, such as retroviruses (Tycowski et al., 2015), encode ncRNAs in the form of microRNAs (miRNAs). These small ncRNAs can be found in most eukaryotic cells and serve to fine-tune the host transcriptome in a sequence-specific manner (Bartel, 2004). Most of the documented virus-encoded miRNAs appear to be involved in establishing persistence (tenOever, 2013). In addition to virus-encoded miRNAs, the increasing sensitivity of deep sequencing technologies has also made it possible to detect other small viral ncRNAs generated from cytoplasmic RNA viruses (Parameswaran et al., 2010; Perez et al., 2010; Shapiro et al., 2010; Weng et al., 2014). While nuclear viruses can use the canonical miRNA biogenesis pathways (Grundhoff and Sullivan, 2011), most RNA viruses induce various alternative cytoplasmic pathways, including cellular or viral factors, to express their ncRNAs (Bidet et al., 2014; Perez et al., 2010). It has been demonstrated that excision of engineered ncRNAs from the viral RNA genome does not result in significant genomic cleavage (tenOever, 2013) or self-induced post-transcriptional gene silencing (Varble et al., 2010). Virus-derived ncRNAs can be functionally relevant in the regulation of the viral life cycle, as demonstrated for influenza virus (Perez et al., 2010) and enterovirus 71 (EV71) (Weng et al., 2014), and also in pathogenesis, as shown for small flavivirus RNAs (Bidet et al., 2014;

Roby et al., 2014). Because growing evidence supports the expression of small ncRNAs by RNA viruses, we wanted to address the question of whether SARS-CoV also generates small ncRNAs during infection.

Here we explore the relevance of viral small ncRNAs in the pathogenesis of SARS-CoV in a mouse model of infection (DeDiego et al., 2007; Roberts et al., 2007). Deep sequencing analysis of small RNAs from the lungs revealed small RNAs from the SARS-CoV genome. Three 18–22 nt small viral RNAs (svRNAs) derived from the nsp3 (svRNA-nsp3.1 and -nsp3.2) and N (svRNA-N) genomic regions of SARS-CoV are characterized. Biogenesis of svRNAs during infection was RNase III independent and modestly impacted viral titers in vitro. Remarkably, depletion of svRNA-N in vivo significantly reduced lung pathology and expression of pro-inflammatory cytokines, supporting that svRNAs contribute to SARS-CoV pathogenesis.

RESULTS

Identification of SARS-CoV-Derived Small Viral RNAs by Deep Sequencing

To address the relevance of small ncRNAs in SARS-CoV pathogenesis, we infected BALB/c mice with either the mouse-adapted virulent SARS-CoV-MA15-WT (Roberts et al., 2007)—which recapitulates infection in humans, including severe lung disease and mortality—or the attenuated SARS-CoV-MA15-ΔE, causing mild lung inflammation (DeDiego et al., 2007). Small RNAs from mouse lung tissue at 2 and 4 days post-infection (dpi) were deep sequenced. Approximately 95% of quality-filtered small RNA sequences mapped to the mouse genome (Table S1), corresponding to the different classes of small cellular RNAs including miRNAs, as previously observed (Peng et al., 2011). Interestingly, small RNA sequences aligning specifically to the SARS-CoV genome were identified at 2 and 4 dpi in the lungs of mice infected with both the virulent SARS-CoV-MA15-WT and the attenuated SARS-CoV-MA15-ΔE, while only residual reads were detected in mock-infected lungs, corresponding to deep sequencing background (Table S1). Sequences that aligned to the SARS-CoV genome represented less than 0.1% of small RNAs, similar to the abundance reported in infections with other RNA viruses (Parameswaran et al., 2010; Perez et al., 2010) and also of SARS-CoV (Peng et al., 2011). Differences in the number of reads between virulent and attenuated SARS-CoV at 2 and 4 dpi demonstrated similar patterns of infectious viral titers in the lung (Figure 1A); lung samples from mice infected with the virulent virus showed the highest number of SARS-CoV-derived reads and viral titer at 2 dpi. A large proportion of svRNAs mapped to the positive-strand genomic RNA (Table S1) and were distributed across the entire viral genome, as expected for viral breakdown products, with an enrichment at the 3′ end of the genome (Figure 1B). In contrast, a limited number of peaks, corresponding to abundant svRNAs mapping to specific genome positions, were also observed (Table S2). In particular, 18% of the viral sequences were enriched for three svRNAs (Table 1) aligning to specific genomic regions in both virulent and attenuated SARS-CoV (Figure 1B) and were selected for further functional studies. These svRNAs were positive sense, 18 to 22 nt in length, and mapped to nsp3 (svRNA-nsp3.1 and svRNA-nsp3.2) at the 5′ end of the Replicase gene

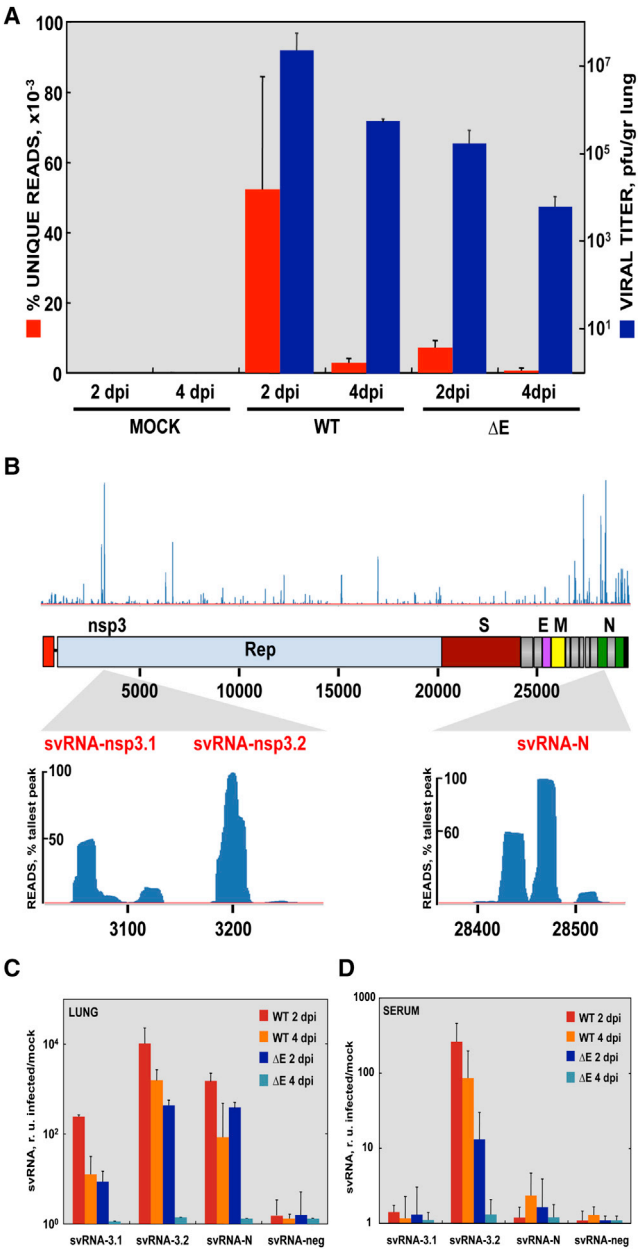

Figure 1. Viral Small RNA Sequences from the SARS-CoV Genome

(A) Percentage of unique reads aligning to the SARS-CoV genome and viral titers from lungs of mock-infected, SARS-CoV-WT (WT), or SARS-CoV-ΔE (ΔE)-infected mice at 2 and 4 dpi.

(B) Representative visual inspection (*Seqmonk* browser) of the small RNA sequences aligning with the SARS-CoV genome. The names of viral genes and the genome positions (nt) are indicated, with detail of the genomic regions, including the three most abundant svRNAs (svRNA-nsp3.1, svRNA-nsp3.2, and svRNA-N), shown under the shadow areas.

(C and D) RT-qPCR detection of svRNA-nsp3.1, svRNA-nsp3.2, and svRNA-N in lungs (C) and serum (D) of infected mice. The viral sequence from nt 3,274–3,295 with no reads detected in deep sequencing was used as negative control (svRNA-neg). Levels of svRNAs were related to those in mock-infected samples, as calculated by the ΔΔCt method using snRNA-U6 and the cel-miR-39 spike as reference endogenous genes in the lung and serum samples, respectively. Data are expressed as means with error bars representing SD. See also Tables 1, S1, and S2.

Table 1. Small Viral RNAs Obtained by Deep Sequencing from SARS-CoV-Infected Lung Tissues

svRNA	Sequence 5′→3′	Genome position	Number of Reads			
			SARS-CoV-wt		SARS-CoV-ΔE	
			2 dpi	4 dpi	2 dpi	4 dpi
nsp3.1	GAGGAAGAAGAGGACGAT	3,052–3,069 nt	386	44	121	23
nsp3.2	GAGGAAGAAGAAGAGGAAGACT	3,184–3,205 nt	832	80	169	33
N	AGGAACTGGCCCAGAAGCTTC	28,461–28,481 nt	706	30	136	17
neg	AATCAGTTTACTGGTTATTTAA	3,274–3,295 nt	0	0	0	0
svRNAs			13.6%	12.09%	22.19%	22.48%

The average number from three biological replicates of all three svRNA reads expressed as the percentage of total reads aligning to the viral genome is indicated in the bottom row for each experimental condition.

and the N gene (svRNA-N) at the 3′ end of the genomic RNA (gRNA). Total reads for each of the three svRNAs were between 17 and 832 (Table 1), with the highest number corresponding to SARS-CoV-MA15-WT infection at 2 dpi, which also showed the highest viral titer (Figure 1A). svRNA-nsp3.1 and svRNA-nsp3.2 shared the first 11 nt of sequence and aligned very close to each other, at positions 3,052 and 3,184 of gRNA, respectively (Figure 1B; Table 1), corresponding to the 5′ and 3′ ends of the Glu-rich acidic hypervariable domain of the nsp3-coding sequence, respectively. In contrast, no reads were detected from a nearby region of nsp3 (3,274–3,295 nt), which was selected as a negative control for further experiments (svRNA-neg). The presence of the three svRNAs and the absence of svRNA-neg in lung samples were confirmed by specific small RNA RT-qPCR assays (Figure 1C). Furthermore, svRNAs were detected to different extents in the serum of SARS-CoV-MA15-WT- and -ΔE-infected mice (Figure 1D), with svRNA-nsp3.2 being the most abundant small RNA in both infections at 2 and 4 dpi. Although the number of svRNA-nsp3.2 and svRNA-N reads in infected lungs were similar (Figure 1C; Table 1), serum levels of svRNA-N were almost the same as in mock-infected mice, suggesting that svRNA-nsp3.2 might be more stable than svRNA-nsp3.1 and svRNA-N in the serum.

Species Specificity in the Induction of SARS-CoV Small RNAs

The kinetics of production of SARS-CoV-derived small RNAs was studied in different mammalian cell lines susceptible to SARS-CoV-MA15-WT infection. In human lung epithelial cells (Calu-3 2B4), svRNA-nsp3.1, -nsp3.2, and -N were detected by RT-qPCR at low levels, in agreement with the lower viral titers obtained in this cell line (Figure S1). In contrast, in mouse DBT-mACE2 cells, the three svRNAs accumulated at high levels, up to a 10^7-fold increase compared to mock-infected cells. As expected, only minimal amounts of svRNA-neg were detected (Figure 2A). A direct correlation was observed between the abundance of svRNAs generated during infection and infectious viral titers or intracellular gRNA amount (Figure 2B), with levels increasing from 24 hr post-infection (hpi) to a maximum at 72 hpi. Moreover, the attenuated SARS-CoV-E-N15A mutant, defective in E protein ion channel activity (Nieto-Torres et al., 2014) and growing as efficiently as the wild-type (WT) virus (Figure S2A), produced in DBT-mACE2 cells similar levels to the WT of svRNAs-nsp3.1, -nsp3.2, and -N (Figure S2B). These results suggested that the generation of svRNA-nsp3.1, -nsp3.2, and -N was not cell or species specific and that it was dependent on the extent of viral replication.

Effect of svRNAs on SARS-CoV Infection in DBT-mACE2 Cells

To address their biological function during SARS-CoV infection, we inhibited svRNAs by transfecting DBT-mACE2 cells with specific anti-svRNA oligonucleotides 24 hr prior to virus infection. The specific inhibition of each svRNA during infection was analyzed by RT-qPCR (Figure 2C). The amounts of svRNA-N were significantly reduced to 5% of the level in cells transfected with a non-related sequence inhibitor (nrRNA) at different time points. Levels of svRNA-nsp3.1 progressively reduced over time although to a lesser extent, with up to 27% of the amount seen in nrRNA-transfected cells. In contrast, transfection with different amounts of specific inhibitor failed to reduce svRNA-nsp3.2 levels. These results may be misleading, since sequence-dependent interference among small RNAs, antisense oligonucleotides, and the qPCR assay has been reported leading to false positive results (Torres et al., 2011); therefore, functional assays were required to confirm svRNA repression. Transfection of increasing doses of svRNA-N inhibitor resulted in a dose-dependent reduction of svRNA-N levels, confirming the specific inhibition of svRNA-N (Figure S3A). Inhibition with anti-svRNAs during infection did not have a significant impact on the levels of nsp3 and N proteins (Figures S3B and S3C). Viral titers in the supernatant were modestly reduced, depending on the time post-infection and the svRNA species (Figure 2D). Inhibition of svRNA-N led to the most significant reduction in comparison with the nrRNA control inhibitor, with more than 1 log unit decrease in viral titers at 72 hpi, whereas inhibition of svRNA-nsp3.1 and -nsp3.2 caused a less significant reduction at the same time point. These results suggest that the production of svRNAs during infection had a positive, although modest, effect on SARS-CoV growth.

Requirements of SARS-CoV svRNA Biogenesis

To determine whether svRNAs were processed by the cell miRNA machinery in the absence of infection, we included 200–500 nt sequences flanking svRNAs in the SARS-CoV genome as potential miRNA precursors within intronic sequences of reporter plasmids (Varble et al., 2010). No processing of viral small RNAs from plasmids was detected (Figure S4), suggesting that svRNA generation was dependent on viral factors or cell proteins induced during virus infection.

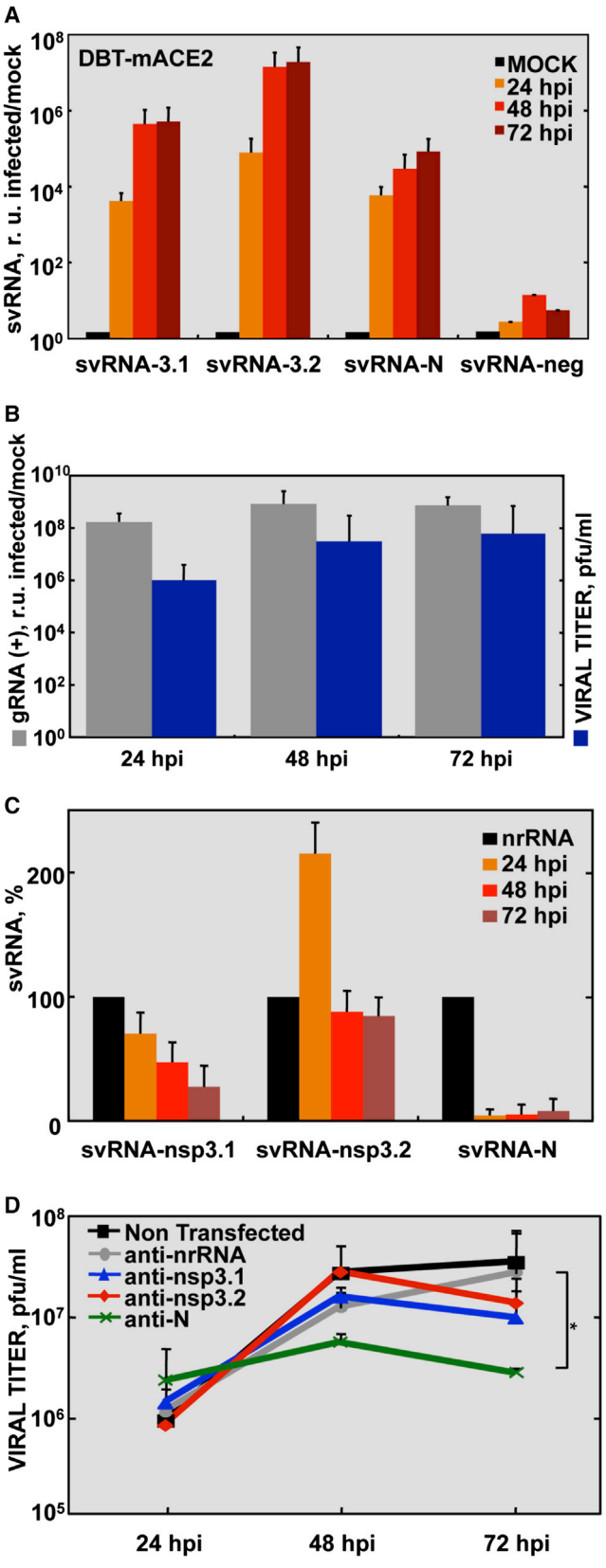

Figure 2. Detection and Functional Analysis of svRNAs in SARS-CoV-Infected DBT-mACE2 Cells

(A) RT-qPCR quantification of svRNA levels at 24, 48, and 72 hpi as indicated in Figure 1.

(B) RT-qPCR quantification of SARS-CoV genomic RNA and viral titers. gRNA levels were related to those in mock-infected cells, as calculated by the ΔΔCt method using *18S rRNA* as a reference endogenous gene. Viral titers were measured from supernatants of infected cells.

(C and D) Inhibition of SARS-CoV-derived svRNAs with RNA inhibitors transfected into DBT-mACE2 cells 24 hr before infection at an MOI = 1; a non-related RNA (nrRNA) was used as a control. (C) svRNA levels determined by qPCR are indicated as a percentage of those in cells transfected with the nrRNA. The ΔΔCt method was used for relative quantification, with snRNA-U6 as an endogenous control. (D) Viral titers after svRNA inhibition. Data are expressed as means with error bars representing SD; *p value < 0.05. See also Figures S1, S2, and S3.

To explore whether svRNAs were generated during SARS-CoV infection by the canonical pathway of miRNA biogenesis, we analyzed svRNA production in absence of the two mammalian RNase III nucleases, Drosha and Dicer, responsible for miRNA processing. 293T and RNase III-deficient cells (Benitez et al, 2015) were made susceptible to SARS-CoV by the transient expression of the murine receptor mACE2 (Regla-Nava et al., 2013). SARS-CoV gRNA levels in RNase III-deficient cells were similar to those of 293T-mACE2, while viral titers were slightly lower in the absence of the RNase III nucleases (Figure 3A), suggesting that these cellular enzymes were not essential for viral replication. Moreover, the biogenesis of svRNAs were not overtly impaired in the absence of Dicer and Drosha suggesting that, should they be miRNAs, the biogenesis pathway responsible for their synthesis was non-canonical (Figure 3B).

Ability of SARS-CoV svRNAs to Repress the Expression of a Target mRNA Reporter

To determine whether svRNAs encoded by SARS-CoV could infer post-transcriptional silencing akin to cellular miRNAs, we cloned the complementary sequence of each svRNA into the 3′ UTR of the luciferase reporter gene, whose activity was measured in the presence or absence of the svRNAs. In a first approach, DBT-mACE2 cells were transfected with oligonucleotides mimicking svRNA-nsp3.1, svRNA-nsp3.2, svRNA-N, or nrRNA along with the appropriate luciferase plasmid in the absence of infection (Figure 4A). All three svRNA mimics repressed luciferase expression, with 40%–60% of the activity measured in the presence of the nrRNA negative control. This repression efficiency was similar to that observed for a mimic of the cellular miR-877-5p, used as positive control. Additionally, co-transfection of inhibitor oligonucleotides with antisense sequence partially (svRNA-nsp3.1) or totally (svRNA-nsp3.2, svRNA-N, and miR-877) restored luciferase activity. In contrast, co-transfection of the inhibitor with a non-related sequence did not affect inhibition of luciferase expression by svRNAs. These results confirm the potential of svRNA-nsp3.1, -nsp3.2, and -N to specifically bind to their target sequences in the 3′ UTR of an mRNA, negatively regulating its expression.

The inhibition of a target mRNA's expression by svRNAs generated in the context of infection would require that the cellular RNA interference (RNAi) machinery remains functional during SARS-CoV infection. To confirm this activity, we

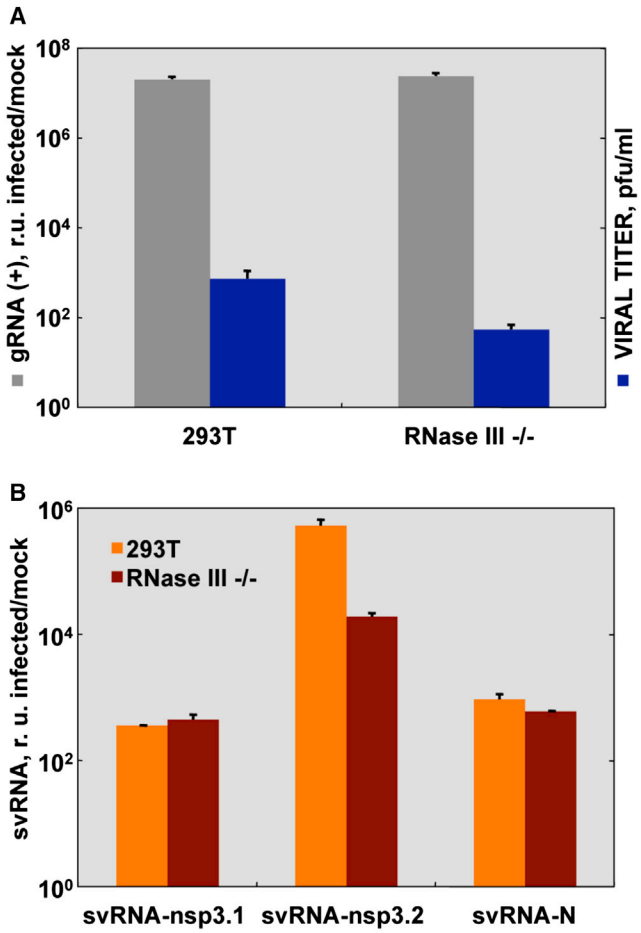

Figure 3. Contribution of the Canonical Cellular miRNA Pathway to the Biogenesis of svRNAs

293T cells and 293T cells deficient in RNase III enzymes Dicer and Drosha (RNase III −/−) were transfected with mACE2 receptor and infected with SARS-CoV at MOI = 5.

(A) Viral gRNA levels in infected cells were analyzed by RT-qPCR and related to those in mock-infected cells, as described in Figure 2. Viral titers were measured from supernatants of infected cells.

(B) svRNAs levels were determined by RT-qPCR and related to those in mock-infected samples, as described in Figure 1. Data are expressed as means with error bars representing SD. See also Figure S4.

transfected the precursor of cellular miR-124 along with a luciferase reporter plasmid containing the miR-124-3p target sequence in the mRNA 3′ UTR. The miR-124-3p that was processed from its precursor sequence efficiently repressed the expression of luciferase to less than 3% of control in both mock and infected cells (Figure 4B), confirming that SARS-CoV infection did not inhibit the cellular RNAi machinery in DBT-mACE2 cells at 24 hpi.

To assess the regulatory effect of svRNAs in infection, we transfected SARS-CoV-infected cells with plasmids encoding luciferase mRNA containing the target sequence of each svRNA in the 3′ UTR (Figure 4C). Only virus-derived svRNA-N significantly silenced luciferase expression as compared to mock-infected cells, although to a lower extent than svRNA-N mimics transfected in the absence of infection (Figure 4C). These results suggest that, although svRNAs per se were able to silence mRNA expression, in the context of infection svRNA-nsp3.1 and svRNA-nsp3.2 may have limited access to the mRNA targets from transfected plasmids either because they are located in different subcellular compartments or because other viral or virus-induced cellular factors competitively inhibit the interaction.

In Vivo Activity of SARS-CoV svRNA-N in the Lungs of Infected Mice

As svRNA-N demonstrated its ability to regulate SARS-CoV growth (Figure 2D) and repress the expression of target mRNAs even in the context of infection in murine cells (Figures 4A and 4C), we selected this svRNA to assess the biological effect in mice, a more relevant system to study potential virus-host interactions (Grundhoff and Sullivan, 2011). To determine the role of svRNA-N in pathogenesis, we used small synthetic RNA molecules perfectly complementary to the specific svRNA, or antagomirs, to inhibit svRNA-N in in vivo SARS-CoV infections. BALB/c mice were intranasally inoculated with a single dose (200 μg) of locked nucleic acids (LNA) corresponding to either anti-svRNA-N or a negative control inhibitor (anti-nrRNA) 24 hr prior to infection with SARS-CoV-MA15-WT. LNAs used in vivo included chemical modifications to increase stability and inhibitory efficacy and to minimize off-target and immunostimulatory effects (Experimental Procedures). No adverse effects, such as weight loss, movement difficulties, lethargy, or unhealthy appearance, were observed in mice after the administration of LNAs over a 10 day follow-up experiment. A significant and lasting reduction of svRNA-N levels to 10% of the non-specific inhibitor control was observed by RT-qPCR at both 2 and 4 dpi (Figure 5A). Mock-infected animals treated with either the svRNA-N inhibitor or the negative control anti-nrRNA did not lose weight throughout the experiment. Inhibition of svRNA-N in SARS-CoV-infected mice was not enough to prevent the weight loss. However, a modest, although sustained, reduction in weight loss was observed in the mice treated with anti-svRNA-N as compared to those treated with the anti-nrRNA over a 7 day period following infection (Figure 5B). svRNA-N inhibition led to a moderate 2-fold reduction in the level of viral gRNA and subgenomic mRNA (sgmRNA)-N at 2 dpi (Figures 5C and 5D), while no significant effect on lung viral titers at that time was observed (Figure 5E), suggesting that svRNA-N had a limited effect in viral replication in vivo.

Lung pathology was examined at 2 and 4 dpi and scored on a severity scale indicating the percentage of affected areas with hemorrhage and pulmonary consolidation (Gralinski et al., 2013). No evident gross lesions were observed in mock-infected lungs. Importantly, svRNA-N inhibition led to a significant reduction in gross pathology (Figures 6A and 6B), in contrast to the lungs of mice treated with the negative control LNA, which showed extensive hemorrhagic areas at 2, and especially at 4, dpi. To further characterize the pulmonary histopathology in SARS-CoV-infected mice treated with the svRNA-N inhibitor, we collected lung sections at 2 and 4 dpi and stained them with hematoxylin and eosin (H&E) (Figure 6C). Pathological features of pulmonary inflammation were scored as previously described (Page et al., 2012) (Figure 6D). Pronounced inflammatory cell infiltration and edema were observed in the alveolar and bronchiolar airways of mice treated with negative control LNA. In

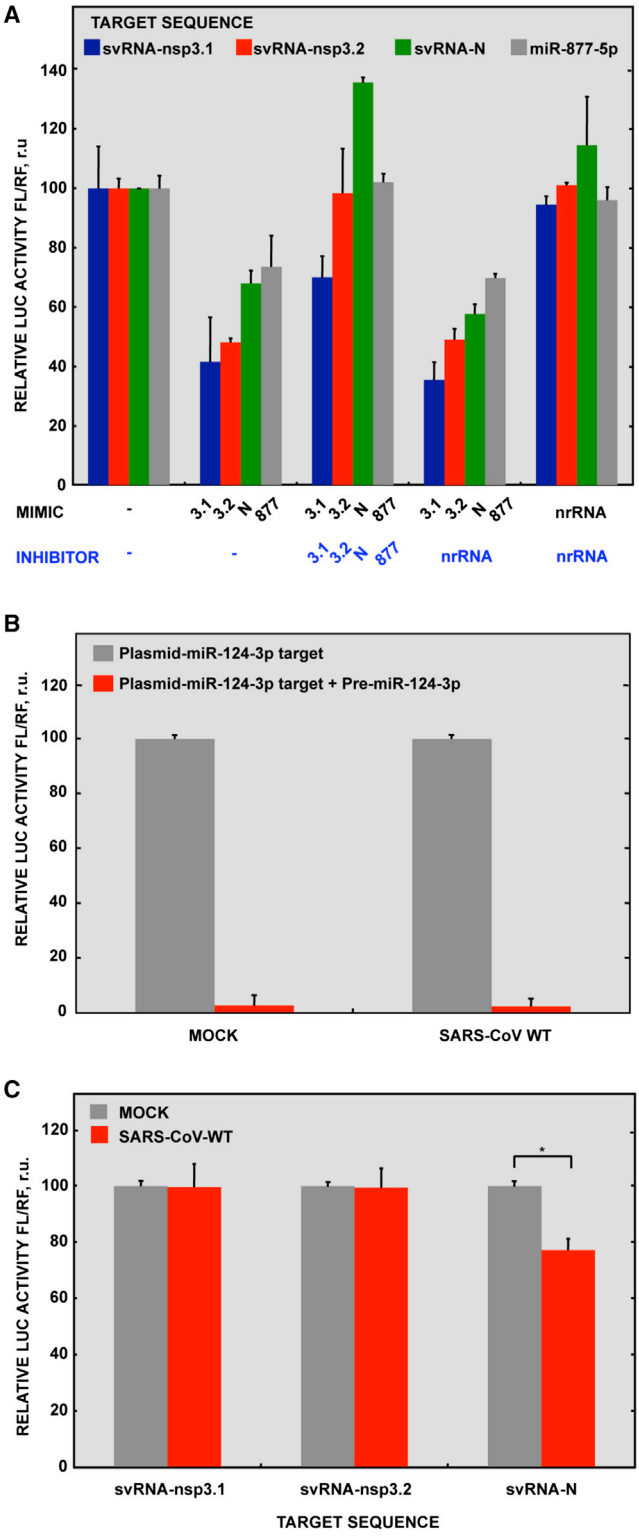

Figure 4. Ability of svRNAs to Repress the Expression of a Reporter mRNA

(A) DBT-mACE2 cells were transfected with luciferase reporter vectors containing the complementary targets for svRNA-nsp3.1, -nsp3.2, and -N in the 3′ UTR. After 6 hr, indicated mimics and inhibitor RNAs of each svRNA were transfected. Cellular miRNA-877-5p was used as a positive control and a non-related viral sequence (nrRNA) as a negative control.

(B) Activity of cellular RNAi pathway in SARS-CoV infection. Relative luciferase activity was measured in mock or SARS-CoV-infected DBT-mACE2 cells transfected with a reporter vector with the target of miR-124-3p in the 3′ UTR of the luciferase gene alone or co-transfected with the miR-124 precursor.

(C) DBT-mACE2 cells were transfected with reporter vectors encoding the complementary targets for svRNA-nsp3.1, -nsp3.2, or -N. At 6 hr post-transfection, cells were mock-infected or infected with SARS-CoV-WT virus. At 24 hpi, relative luciferase activity was measured. Data are expressed as means with error bars representing SD; *p value < 0.05.

contrast, the treatment with anti-svRNA-N significantly reduced inflammation, keeping alveolar spaces free, and—as a consequence—also improved animal welfare.

SARS-CoV infection induces high levels of pro-inflammatory cytokines, which contribute to lung immunopathology and promote SARS-CoV morbidity and mortality (Channappanavar et al., 2016; DeDiego et al., 2014). To study whether treatment with anti-svRNA-N LNA affected the production of pro-inflammatory cytokines in the lungs, we analyzed the expression of several genes previously associated with SARS-CoV pathology, including *CCL2*, *IL-6*, and *CXCL10* (Jimenez-Guardeño et al., 2014). A significant decrease in the mRNA expression levels of *CCL2*, *IL-6*, and *CXCL10* was observed in mice treated with the svRNA-N inhibitor (Figure 6E), in agreement with the observed reduction in lung pathology. Moreover, inhibition of svRNA-N significantly increased the expression of antiviral interferon (IFN) stimulated genes, such as *ISG15* and *MX1*. In contrast, no significant effect was observed on *IFN-γ*, indicating specificity in the effect of svRNA-N on the expression of pro-inflammatory cytokines. Since the inhibition of svRNA-N did not affect viral titers in the lungs (Figure 5E), the observed decrease in inflammation should not be attributed to a reduction in viral growth. Overall, these results showed a contribution of svRNAs to the inflammatory lung pathology induced by SARS-CoV infection.

To address the question of tissue specificity of svRNA-N action, we performed immunohistochemistry staining of infected lung tissue at days 2 and 4 post-infection. Lungs from mice treated with svRNA-N inhibitor showed staining for SARS-CoV both in the bronchiolar airways and in the lung parenchyma similar to the tissue distribution observed in the animals treated with the negative control inhibitor (Figure S5). These results confirmed that inhibition of svRNA-N reduced inflammatory cell infiltration and edema in the lung, with no significant effect on the tissue specificity of SARS-CoV infection.

DISCUSSION

We have studied the relevance in SARS-CoV pathogenesis of small ncRNAs derived from the viral genome. Small RNAs were analyzed by deep sequencing from the lungs of SARS-CoV-MA15-infected BALB/c mice, which reproduce the severe pulmonary disease observed in humans during SARS-CoV epidemics (Roberts et al., 2007). Since ncRNAs are cell specific, it is expected that this in vivo approach provides biologically relevant results in terms of their contribution to virus-host interaction (Cox and Sullivan, 2014).

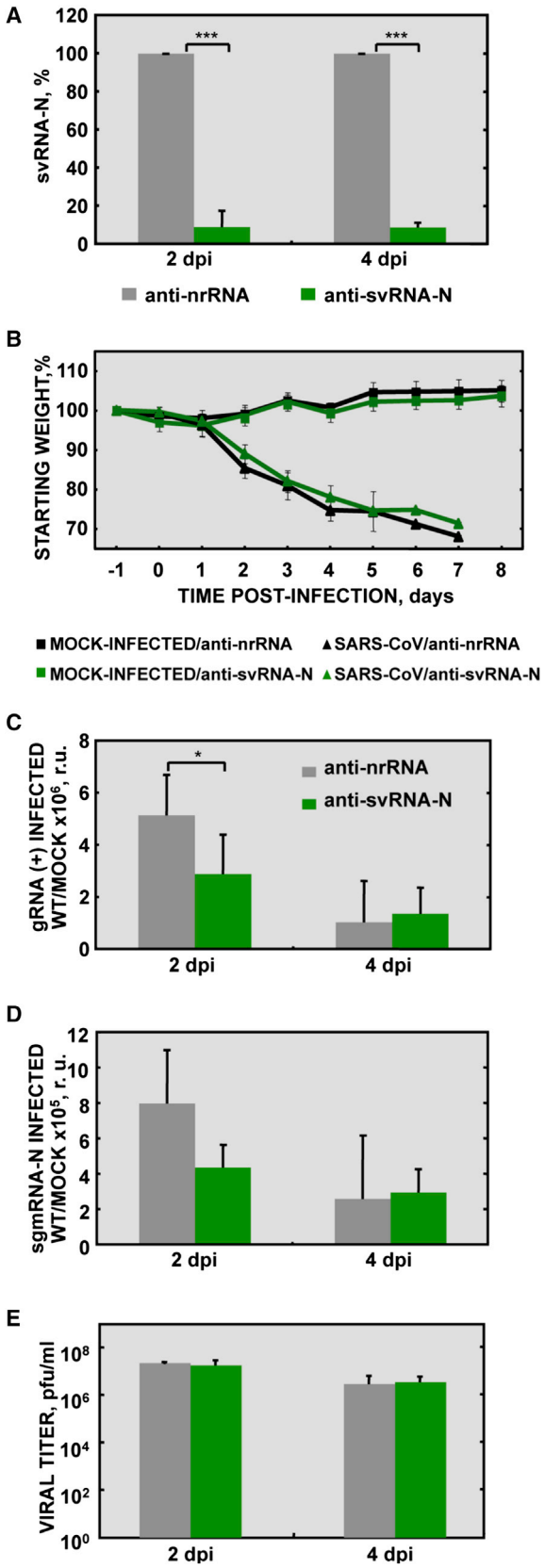

Figure 5. Functional Analysis of svRNA-N in SARS-CoV-Infected Mice Using LNA RNA Inhibitors

BALB/c mice were intranasally inoculated with 200 μg (10 mg/kg) of the LNA svRNA-N inhibitor or non-related sequence (nrRNA) as a negative control. After 24 hr, the mice were infected with 10^5 PFU of SARS-CoV, and their lungs were collected at 2 and 4 dpi.

(A) RT-qPCR analysis of svRNA-N relative expression in the lungs, indicated as a percentage of the expression in mice inoculated with nrRNA. The ΔΔCt method was used for relative quantification, as described in Figure 1; ***p value < 0.001.

(B) Average weight of mice over an 8 day period after SARS-CoV infection (day 0), expressed as a percentage of the initial weight. Day −1, inoculation of inhibitor. At least five mice were weighted daily.

(C) Level of SARS-CoV gRNA in infected mice treated with svRNA inhibitors determined by RT-qPCR. The ratio of gRNA (+) in infected to mock-infected lungs is represented, as described in Figure 2; *p value < 0.1.

(D) Levels of sgmRNA-N determined by RT-qPCR and calculated as described in (C).

(E) Viral titers in the lungs of SARS-CoV-infected mice treated with the svRNA-N inhibitor. Data are expressed as means with error bars representing SD. Figure legends in (D) and (E) are the same as in (C).

This analysis resulted in the discovery of small RNAs derived from SARS-CoV. There is growing evidence supporting the generation of small ncRNAs from RNA viruses, as described in influenza virus (Perez et al., 2010), EV71 (Weng et al., 2014), hepatitis A virus (HAV) (Shi et al., 2014), HCV, Polio, Dengue, vesicular stomatitis, and West Nile viruses (Parameswaran et al., 2010). As described for other RNA viruses, such as HAV (Shi et al., 2014) and influenza (Perez et al., 2010), svRNAs represent a minor proportion (<0.1%) of total small RNA sequences obtained from infected tissues, although this low abundance is compatible with a relevant biological function. In the current work, the abundance of SARS-CoV-derived svRNAs was correlated with viral titers, as observed in several experimental systems (Figures 1A and 2). Furthermore, as observed with other RNA viruses, the vast majority of SARS-CoV svRNA sequences were positive sense, the same as the viral genome (Parameswaran et al., 2010; Shi et al., 2014). The svRNAs were not evenly distributed throughout the SARS-CoV genome, suggesting production from "hotspots" located preferentially near the genome ends. This pattern was also observed in influenza virus (Perez et al., 2010) and argues that these svRNAs are not merely viral degradation products, but that they are actively generated and play a role during infection (Perez et al., 2012). The three most abundant svRNAs represented 18% of the total viral sequences and aligned to SARS-CoV genomic regions expressed at different levels during infection. Two of them, svRNA-nsp3.1 and -nsp3.2, were generated from the genomic region coding for the nsp3 Glu-rich acidic domain. Nsp3 is one of the non-structural proteins produced by the proteolytic processing of the Replicase polyprotein. Nsp3 is the largest Replicase subunit (1,922 aa) with a multi-domain structure including transmembrane domains, the papaine-like protease domain, a nucleic-acid binding domain, ubiquitin-like domains, a Glu-rich acidic domain, an ADP-ribose-1″-phosphatase domain (ADRP or macrodomain or X domain), and a SARS-unique domain (SUD) (Báez-Santos et al., 2015; Neuman et al., 2008). svRNAs nsp3.1 and nsp3.2 map to the 5′ and 3′ ends of the Glu-rich acidic hypervariable coding region, respectively. This domain has been involved in interactions with single-stranded RNA. The Replicase gene is expressed at lower levels than the 3′-most genomic region, which is present

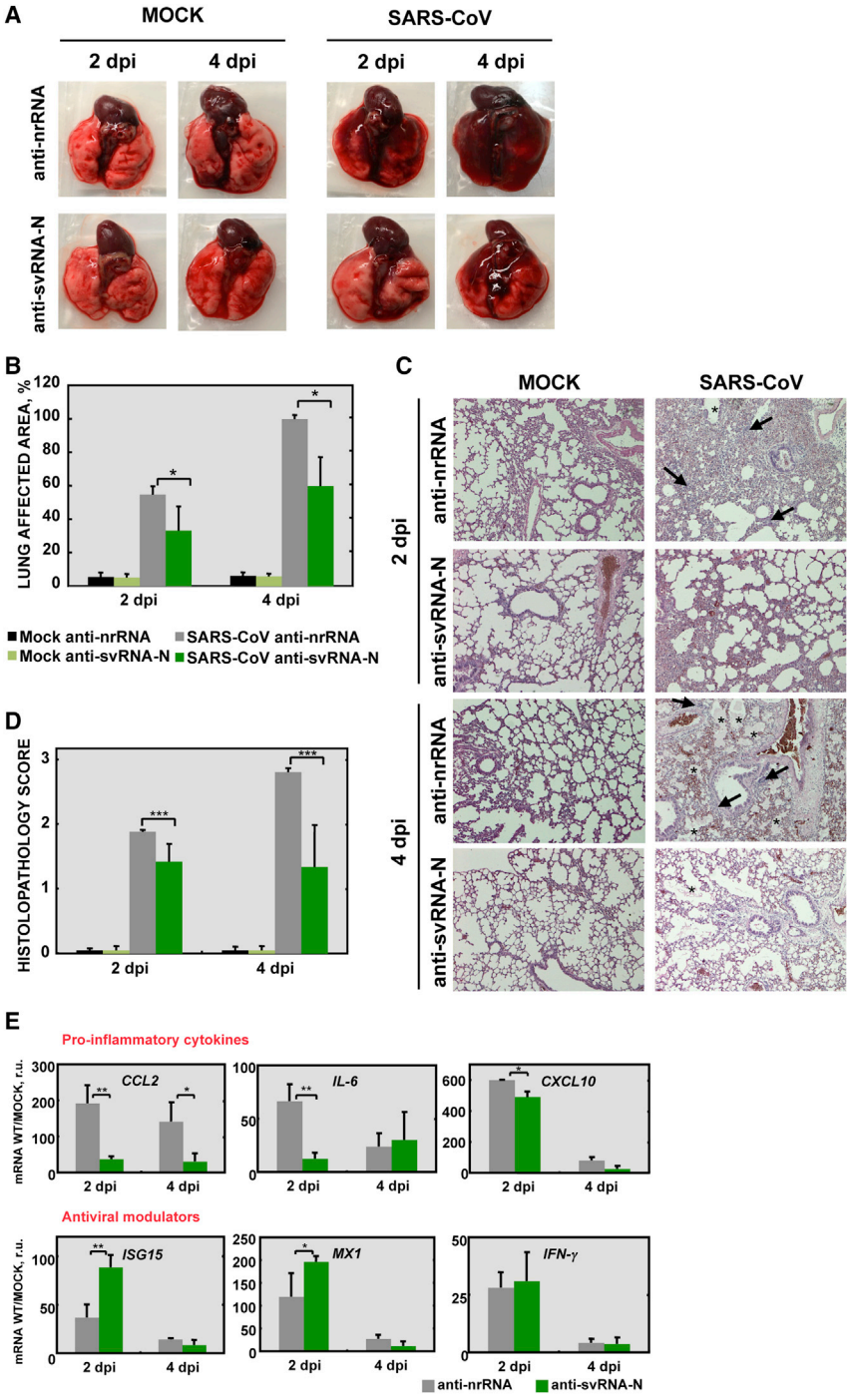

Figure 6. Lung Pathology in SARS-CoV-Infected Mice Using LNA RNA Inhibitor of svRNA-N

(A) Gross pathology of lungs from mock- and SARS-CoV-infected mice treated with either the LNA svRNA-N (anti-svRNA-N) or the negative control inhibitor (nrRNA).

(B) Gross pulmonary pathology was scored in a blinded fashion (L.M.) for three animals per condition on a severity scale indicating the percentage of affected areas showing hemorrhage and pulmonary consolidation (Gralinski et al., 2013).

(C) Histopathological analysis at 2 and 4 days post-infection of hematoxylin and eosin-stained lung sections from mice treated as in (A). Images are representative of 50 microscopy fields observed for each of the three independent mice analyzed per treatment group; arrows indicate cell infiltrates and asterisks indicate edema.

(D) Histopathology scoring of lungs from infected mice treated with the svRNA-N inhibitor. Lung samples were analyzed (L.M.) in a blind manner, using a severity scale from 0 (absent) to 3 (severe with presence of interstitial, peribronchiolar, and perivascular inflammation) (Page et al., 2012); ***p value < 0.001. Figure legends in (D) are the same as in (B).

(E) qPCR determination of mRNA levels for the indicated inflammatory mediators. The ratio of mRNA in infected to mock-infected lungs is indicated, as calculated by the ΔΔCt method using *18S rRNA* as an endogenous control. Data are expressed as means with error bars representing SD; *p value < 0.1, **p value < 0.01. See also Figure S5.

in a collection of 3′ co-terminal sgmRNAs generated by discontinuous transcription (Enjuanes et al., 2008). The svRNA-N, derived from the N gene located at the 3′ end of the genome, was expressed at significantly higher levels than background from surrounding viral sequences. Coronavirus nucleoprotein N is essential for the formation of the virion structure and also for RNA synthesis. It has been shown that CoV N protein has RNA chaperone activity, which is required for efficient discontinuous transcription of subgenomic RNAs (Zúñiga et al., 2010). svRNA-N maps to the N gene-structured region coding for the RNA-binding domain, which is located at the N terminus of the protein, preceding a disordered central region. svRNA-nsp3.1 and svRNA-nsp3.2 share the first 11 nt of sequence. This sequence (5′-GAGGAAGAAGA-3′) is repeated three times in the SARS-CoV genome at positions 3,052, 3,079, and 3,184 within the region coding for the nsp3 Glu-rich domain. svRNA-nsp3.1 and -nsp3.2 derived from genomic sequences starting at nt 3,052 and 3,184, while the sequence at nt 3,079 did not produce a significant number of reads (<75). The relevance of these repeated GA-rich motifs in the generation of svRNAs would require further investigation. High levels of svRNA-nsp3.2 were also detected in the serum of infected mice, while svRNA-nsp3.1 and -N were not present at significant levels despite their similar abundance in the lungs. This observation may reflect relative stability or, alternatively, may suggest that svRNA-nsp3.2 may be actively transported to the blood. The presence of svRNA-nsp3.2 in the serum was common in both WT and SARS-CoV-ΔE infections, suggesting that the mechanisms responsible for the specific transport to the blood do not depend on E protein activity.

The three SARS-CoV svRNAs are all derived from coding regions of the genome, as observed in other RNA viruses, such as HAV (Shi et al., 2014). In contrast, svRNAs from influenza virus are derived from the 5′ non-coding region of each segment (Perez et al., 2010). A theoretical argument against svRNAs derived from cytoplasmic RNA viruses was that their excision was deleterious to viral genome integrity (Cullen, 2011). However, cytoplasmic viruses have been engineered, producing functional miRNAs from their genome with no significant impact on viral growth (Bidet et al., 2014; Varble et al., 2010; Weng et al., 2014; Shapiro et al., 2010). Our results show that inhibition with anti-svRNAs during infection did not have a significant impact on the levels of nsp3 and N proteins, suggesting that no important loss of genomic material or interference with the replication machinery were induced as a consequence of svRNA production. svRNAs are perfectly complementary to negative-sense replication intermediate RNAs, which might be self-silencing targets. However, svRNA inhibition did not increase the expression of viral proteins nsp3 and N or viral titers, suggesting that svRNAs did not have a relevant gene-silencing activity on negative-sense SARS-CoV RNAs.

Our results support that the biogenesis of SARS-CoV svRNAs was mainly independent of canonical cellular pathways and dependent on alternative mechanisms involving viral proteins or cellular factors induced during infection, since mature 18–22 nt svRNA species were not generated in non-infected cells from plasmids that included viral genomic sequences. Biogenesis of svRNAs was independent of miRNA processing enzymes Dicer and Drosha. These results suggest that biogenesis may require Argonaute 2 as in the case for miR-451 (Cheloufi et al., 2010) or be generated by a viral nuclease. CoV Replicase encodes some essential RNA-processing enzymes not found in other RNA virus families, such as the Endoribonuclease (nsp15) (Ricagno et al., 2006), which might be involved in the biogenesis of svRNAs from the SARS-CoV genome. Nsp15 has nucleolytic activity in both single- and double-stranded RNA, although its specific function in RNA synthesis is not completely understood. The production of specific small viral RNAs from viral components has been demonstrated for influenza virus (Perez et al., 2010). Alternatively, non-coding subgenomic flavivirus RNA is generated by the cellular 5′–3′ Exoribonuclease XRN1, which partially degrades the genomic RNA stalling at secondary RNA structures at the 3′ UTR (Roby et al., 2014). Although the number of examples for svRNAs expressed by RNA viruses is still limited, a variety of mechanisms have been involved in their biogenesis and function. In general, these svRNAs are generated from the genome ends or nearby regions (Perez et al., 2010; Weng et al., 2014; Roby et al., 2014). In SARS-CoV, svRNAs are generated from more internal genomic regions, although relatively close to the 5′ (svRNA-nsp3.1 and -nsp3.2) or 3′ (svRNA-N) ends, considering that SARS-CoV has one of the largest genomes (around 29,600 nt) among RNA viruses. Differences in the genomic origin of svRNAs in SARS-CoV as compared to other RNA viruses might be explained by the heterogeneity in biogenesis and mechanisms of action.

Regarding their function, viral ncRNAs could contribute to the regulation of the viral life cycle (Perez et al., 2010; Weng et al., 2014) or to inhibit host defenses against viral infection (Ding and Voinnet, 2007). Loss-of-function studies of SARS-CoV svRNAs using antisense oligonucleotides in DBT-mACE2 cells only showed a significant reduction in virus titers at late times post-infection for svRNA-N, associated with a reduction in svRNAs levels, suggesting that svRNAs did not have a relevant contribution to virus replication. To analyze the biological relevance of SARS-CoV svRNA-N, we studied its function in vivo, providing a physiological context for virus-host interactions, including the innate immune response and the RNA-mediated regulatory network. Inhibition of svRNA-N in vivo only reduced moderately the accumulation of gRNA in the lungs of infected mice at 2 dpi, with no significant decrease in viral titers, suggesting that the effect of svRNA-N on viral replication was not relevant.

Remarkably, administration of anti-svRNA-N LNAs prior to infection with SARS-CoV reduced pulmonary inflammation and production of pro-inflammatory cytokines in mice, although viral titers were not significantly affected. A moderate reduction in lung damage markers—such as edema and cellular infiltrates—observed at 2 and 4 dpi, and the reduction in pro-inflammatory cytokines—such as *CCL2*, *IL-6*, and *CXCL10*—support a contribution of svRNAs to inflammatory lung pathogenesis. Moreover, inhibition of svRNA-N increased the expression at 2 dpi of *ISG15* and *MX1*, which are modulators of the host response to viral infections. Inhibition of svRNA-N in vivo supports the contribution of ISGs (ISG15 and MX1) to lung pathology as immunomodulatory molecules reducing potentially pathologic levels of pro-inflammatory molecules rather than having a direct antiviral effect. Similarly, depletion of ISG15 in Chikungunya virus-infected mice has been shown to promote an increase in pro-inflammatory cytokines without affecting viral titers (Werneke et al., 2011). svRNA-N-induced reduction of inflammatory pathology was not associated with decrease in viral titers. These results were in agreement with prior observations in SARS-CoV-infected humans and animals indicating that the major mechanism of lung pathogenesis was the dysregulated and excessive expression of several pro-inflammatory cytokines and chemokines, which was independent of the extent of virus replication, naturally after a minimum threshold of virus replication has been achieved (Nicholls et al., 2003; Channappanavar et al., 2016; Jimenez-Guardeño et al., 2014; Nieto-Torres et al., 2014). During infection, svRNA-N may act via cellular factors, either through RNA-RNA interactions as known for miRNAs or by RNA-protein interactions (Bidet et al., 2014; Perez et al., 2010). Since svRNA-N was able to silence the expression of a target mRNA reporter (Figure 4), we propose that it might contribute to lung pathology (Figure 6) by regulating cellular mRNAs involved in the host inflammatory response via the RNAi. svRNA expression might increase inflammation by repressing the expression of factors involved in the downregulation of the host inflammatory response. Unfortunately, current knowledge about the mechanism of action of svRNAs is still very limited, with no information on whether they bind their targets through a seed sequence (and thus repress expression similarly to canonical miRNAs), making the bioinformatic prediction of targets a complex objective.

The genomic sequences in the mouse-adapted SARS-CoV-MA15 from which svRNAs originate are conserved in the human

SARS-CoV (Urbani strain) and in other SARS-related bat CoVs, including LYRa11, RF1, Rm1, Rs3367, and Cp/Yunnan 2011 isolates, but not in more distant CoVs, such as MERS-CoV, suggesting some genus specificity. In particular, svRNA-N is completely conserved in SARS-related bat CoVs. Therefore, infection with the human SARS-CoV would also be expected to generate svRNAs identical to those originated from SARS-CoV-MA15. Providing that svRNAs act by binding to complementary sequences in target mRNAs, svRNAs from the human or the mouse-adapted SARS-CoV might be expected to regulate the expression of human or mouse mRNAs in a similar manner, since miRNA targets in 3′ UTR of mammalian mRNAs are preferentially conserved (Friedman et al., 2009).

As svRNA-N inhibition reduced lung pathology caused by SARS-CoV, anti-svRNA-N is a potentially useful compound for antiviral therapy, although it was not sufficient to increase mice survival, possibly because the dose and schedule of administration of LNA anti-svRNA-N need to be optimized. Moreover, SARS-CoV includes many virulence factors, such as the E protein, that promote inflammation by different mechanisms (Jimenez-Guardeño et al., 2014). The attenuated SARS-CoV-E-N15A mutant, defective in E protein ion channel activity, grew as efficiently as the WT virus (Nieto-Torres et al., 2014) and produced similar levels of svRNAs-nsp3.1, -nsp3.2, and -N in DBT-mACE2 cells. If we assume that svRNA production in vivo is also comparable for both viruses, then svRNA-N might be contributing to the limited pro-inflammatory response still present in SARS-CoV-E-N15A-infected mice as compared to non-infected mice, confirming that multiple mechanisms are contributing to the SARS-CoV lung pathology. The use of antagomirs as antivirals has several advantages compared to other strategies: high specificity against virus-derived targets, avoidance of secondary effects by action on cellular targets, and ability to be used in combination with other antiviral therapies to increase efficacy and safety. In fact, LNA-anti-miR-122 has been administrated in humans with promising efficacy in reducing HCV RNA (Janssen et al., 2013). Unraveling the molecular mechanism of svRNA-N contributing to lung inflammation will aid in the design of antivirals to control the exacerbated host response induced by SARS-CoV infection.

EXPERIMENTAL PROCEDURES

Ethics Statement

Animal experimental protocols were approved by the Ethical Committee of the Center for Animal Health Research (CISA-INIA) (permit numbers: 2011–009 and 2011–09) in strict accordance with Spanish National Royal Decree (RD 1201/2005) and international EU guidelines 2010/63/UE about protection of animals used for experimentation and other scientific purposes and Spanish Animal Welfare Act 32/2007. All work with infected animals was performed in a BSL3 laboratory of the Center for Animal Health Research (CISA-INIA).

Viruses and Cell Lines

The mouse-adapted (MA15) (Roberts et al., 2007) parental SARS-CoV and recombinant SARS-CoV-ΔE and SARS-CoV-E-N15A viruses were rescued from infectious cDNA clones generated in bacterial artificial chromosomes (BAC) in our laboratory (DeDiego et al., 2007; Nieto-Torres et al., 2014). Cell lines were generated and maintained as described in Supplemental Experimental Procedures. Cells deficient in Dicer and Drosha are described elsewhere (Benitez et al., 2015). Virus titrations were performed in Vero E6 cells as described in Supplemental Experimental Procedures.

In Vivo Infections

16-week-old female mice were intranasally inoculated with 10^5 PFU of rSARS-CoV-WT or rSARS-CoV-ΔE. For the svRNA-N inhibition experiment, 24 hr prior to infection, mice were intranasally inoculated with 200 μg (10 mg/kg) of the inhibitor (miRCURY LNA microRNA Inhibitor, Exiqon). For intranasal inoculations, mice were lightly anesthetized with isoflurane, and then 50 μL of solution containing either the svRNA inhibitor (24 hr before infection) or the virus were laid on the nostrils of the mouse using a pipette tip. The small droplet was naturally inhaled by the mouse about 2–3 s later. Since this procedure is non-invasive and does not require a relevant physical intervention, it did not cause any inflammation in the mice.

Lung Samples from SARS-CoV-Infected Mice

To analyze SARS-CoV titers, we homogenized one-quarter of the right lung in 2 mL of phosphate-buffered saline (PBS) containing 100 UI/mL penicillin, 100 μg/mL streptomycin, 50 μg/mL gentamicin, and 0.5 μg/mL fungizone using a MACS homogenizer (Miltenyi Biotec) according to manufacturer's protocols and performed virus titrations as described in Supplemental Experimental Procedures. To isolate long and small RNAs separately, we homogenized one-half of the right lung in 2 mL of Lysis/Binding Solution (mirVana miRNA Isolation Kit, Ambion) using a MACS homogenizer (Miltenyi Biotec) according to manufacturer's protocols and extracted RNA using mirVana miRNA Isolation protocol for isolation of small RNAs from total RNA samples. To examine lung histopathology, we fixed the left lung of infected mice in 10% zinc formalin for 24 hr at 4°C and embedded it in paraffin. Serial longitudinal 5 μm sections were stained with H&E by the Histology Service in the National Center of Biotechnology (CNB, Spain) and subjected to histopathological examination with a ZEISS Axiophot fluorescence microscope. Samples were obtained using a systematic uniform random procedure, consisting in serial parallel slices made at a constant thickness interval of 50 μm. Histopathology analysis was conducted in a blind manner by acquiring images of 50 random microscopy fields from around 40 non-adjacent sections for each of the three independent mice analyzed per treatment group. The measurement of lung damage was scored using a severity scale from 0 (absent) to 3 (severe with presence of interstitial, peribronchiolar, and perivascular inflammation) as described (Page et al., 2012).

ACCESSION NUMBERS

The accession number for small RNA sequencing raw data reported in this paper is GEO: GSE90624.

SUPPLEMENTAL INFORMATION

Supplemental Information includes Supplemental Experimental Procedures, five figures, and two tables and can be found with this article online at http://dx.doi.org/10.1016/j.chom.2017.01.015.

AUTHOR CONTRIBUTIONS

L.M. designed and performed the experiments, analyzed the data, and wrote the manuscript; J.C.O. developed bioinformatics tools and analyzed the data; R.F.-D. designed and performed the experiments; B.R.T. provided reagents and conceptual advice and wrote the manuscript; L.E. and I.S. conceived the project, designed the experiments, and wrote the manuscript.

ACKNOWLEDGMENTS

This work was supported by grants from the Ministry of Science and Innovation of Spain (BIO2010-16705, BIO2013-42869-R, and BIO2016-75549-R AEI/FEDER, UE), the European Zoonoses anticipation and preparedness initiative ZAPI (IMI_JU_115760), and U.S. National Institutes of Health (NIH) (2P01AI060699 and 0258-3413/HHSN266200700010C). L.M. received a fellowship from the Ministry of Science an Innovation of Spain (BIO2010-16705) and a contract from ZAPI. R.F.-D received contracts from NIH and ZAPI.

Received: July 14, 2016
Revised: December 20, 2016
Accepted: January 25, 2017
Published: February 16, 2017

REFERENCES

Báez-Santos, Y.M., St John, S.E., and Mesecar, A.D. (2015). The SARS-coronavirus papain-like protease: structure, function and inhibition by designed antiviral compounds. Antiviral Res. *115*, 21–38.

Bartel, D.P. (2004). MicroRNAs: genomics, biogenesis, mechanism, and function. Cell *116*, 281–297.

Benitez, A.A., Spanko, L.A., Bouhaddou, M., Sachs, D., and tenOever, B.R. (2015). Engineered mammalian RNAi can elicit antiviral protection that negates the requirement for the interferon response. Cell Rep. *13*, 1456–1466.

Bidet, K., Dadlani, D., and Garcia-Blanco, M.A. (2014). G3BP1, G3BP2 and CAPRIN1 are required for translation of interferon stimulated mRNAs and are targeted by a dengue virus non-coding RNA. PLoS Pathog. *10*, e1004242.

Channappanavar, R., Fehr, A.R., Vijay, R., Mack, M., Zhao, J., Meyerholz, D.K., and Perlman, S. (2016). Dysregulated type I interferon and inflammatory monocyte-macrophage responses cause lethal pneumonia in SARS-CoV-infected mice. Cell Host Microbe *19*, 181–193.

Cheloufi, S., Dos Santos, C.O., Chong, M.M., and Hannon, G.J. (2010). A dicer-independent miRNA biogenesis pathway that requires Ago catalysis. Nature *465*, 584–589.

Cox, J.E., and Sullivan, C.S. (2014). Balance and stealth: the role of noncoding RNAs in the regulation of virus gene expression. Annu Rev Virol *1*, 89–109.

Cullen, B.R. (2011). Viruses and microRNAs: RISCy interactions with serious consequences. Genes Dev. *25*, 1881–1894.

DeDiego, M.L., Alvarez, E., Almazán, F., Rejas, M.T., Lamirande, E., Roberts, A., Shieh, W.J., Zaki, S.R., Subbarao, K., and Enjuanes, L. (2007). A severe acute respiratory syndrome coronavirus that lacks the E gene is attenuated in vitro and in vivo. J. Virol. *81*, 1701–1713.

DeDiego, M.L., Nieto-Torres, J.L., Regla-Nava, J.A., Jimenez-Guardeño, J.M., Fernandez-Delgado, R., Fett, C., Castaño-Rodriguez, C., Perlman, S., and Enjuanes, L. (2014). Inhibition of NF-κB-mediated inflammation in severe acute respiratory syndrome coronavirus-infected mice increases survival. J. Virol. *88*, 913–924.

Ding, S.W., and Voinnet, O. (2007). Antiviral immunity directed by small RNAs. Cell *130*, 413–426.

Enjuanes, L., Gorbalenya, A.E., de Groot, R.J., Cowley, J.A., Ziebuhr, J., and Snijder, E.J. (2008). The Nidovirales. In Encyclopedia of Virology, Third Edition, B.W.J. Mahy, M. Van Regenmortel, P. Walker, and D. Majumder-Russell, eds. (Elsevier Ltd.), pp. 419–430.

Friedman, R.C., Farh, K.K., Burge, C.B., and Bartel, D.P. (2009). Most mammalian mRNAs are conserved targets of microRNAs. Genome Res. *19*, 92–105.

Gralinski, L.E., Bankhead, A., 3rd, Jeng, S., Menachery, V.D., Proll, S., Belisle, S.E., Matzke, M., Webb-Robertson, B.J., Luna, M.L., Shukla, A.K., et al. (2013). Mechanisms of severe acute respiratory syndrome coronavirus-induced acute lung injury. MBio *4*, e00271–e00213.

Grundhoff, A., and Sullivan, C.S. (2011). Virus-encoded microRNAs. Virology *411*, 325–343.

Janssen, H.L., Reesink, H.W., Lawitz, E.J., Zeuzem, S., Rodriguez-Torres, M., Patel, K., van der Meer, A.J., Patick, A.K., Chen, A., Zhou, Y., et al. (2013). Treatment of HCV infection by targeting microRNA. N. Engl. J. Med. *368*, 1685–1694.

Jimenez-Guardeño, J.M., Nieto-Torres, J.L., DeDiego, M.L., Regla-Nava, J.A., Fernandez-Delgado, R., Castaño-Rodriguez, C., and Enjuanes, L. (2014). The PDZ-binding motif of severe acute respiratory syndrome coronavirus envelope protein is a determinant of viral pathogenesis. PLoS Pathog. *10*, e1004320.

Neuman, B.W., Joseph, J.S., Saikatendu, K.S., Serrano, P., Chatterjee, A., Johnson, M.A., Liao, L., Klaus, J.P., Yates, J.R., 3rd, Wüthrich, K., et al. (2008). Proteomics analysis unravels the functional repertoire of coronavirus nonstructural protein 3. J. Virol. *82*, 5279–5294.

Nicholls, J.M., Poon, L.L., Lee, K.C., Ng, W.F., Lai, S.T., Leung, C.Y., Chu, C.M., Hui, P.K., Mak, K.L., Lim, W., et al. (2003). Lung pathology of fatal severe acute respiratory syndrome. Lancet *361*, 1773–1778.

Nieto-Torres, J.L., DeDiego, M.L., Verdiá-Báguena, C., Jimenez-Guardeño, J.M., Regla-Nava, J.A., Fernandez-Delgado, R., Castaño-Rodriguez, C., Alcaraz, A., Torres, J., Aguilella, V.M., and Enjuanes, L. (2014). Severe acute respiratory syndrome coronavirus envelope protein ion channel activity promotes virus fitness and pathogenesis. PLoS Pathog. *10*, e1004077.

Page, C., Goicochea, L., Matthews, K., Zhang, Y., Klover, P., Holtzman, M.J., Hennighausen, L., and Frieman, M. (2012). Induction of alternatively activated macrophages enhances pathogenesis during severe acute respiratory syndrome coronavirus infection. J. Virol. *86*, 13334–13349.

Parameswaran, P., Sklan, E., Wilkins, C., Burgon, T., Samuel, M.A., Lu, R., Ansel, K.M., Heissmeyer, V., Einav, S., Jackson, W., et al. (2010). Six RNA viruses and forty-one hosts: viral small RNAs and modulation of small RNA repertoires in vertebrate and invertebrate systems. PLoS Pathog. *6*, e1000764.

Peng, X., Gralinski, L., Ferris, M.T., Frieman, M.B., Thomas, M.J., Proll, S., Korth, M.J., Tisoncik, J.R., Heise, M., Luo, S., et al. (2011). Integrative deep sequencing of the mouse lung transcriptome reveals differential expression of diverse classes of small RNAs in response to respiratory virus infection. MBio *2*, e00198–e00111.

Perez, J.T., Varble, A., Sachidanandam, R., Zlatev, I., Manoharan, M., García-Sastre, A., and tenOever, B.R. (2010). Influenza A virus-generated small RNAs regulate the switch from transcription to replication. Proc. Natl. Acad. Sci. USA *107*, 11525–11530.

Perez, J.T., Zlatev, I., Aggarwal, S., Subramanian, S., Sachidanandam, R., Kim, B., Manoharan, M., and tenOever, B.R. (2012). A small-RNA enhancer of viral polymerase activity. J. Virol. *86*, 13475–13485.

Perlman, S., and Netland, J. (2009). Coronaviruses post-SARS: update on replication and pathogenesis. Nat. Rev. Microbiol. *7*, 439–450.

Regla-Nava, J.A., Jimenez-Guardeño, J.M., Nieto-Torres, J.L., Gallagher, T.M., Enjuanes, L., and DeDiego, M.L. (2013). The replication of a mouse adapted SARS-CoV in a mouse cell line stably expressing the murine SARS-CoV receptor mACE2 efficiently induces the expression of proinflammatory cytokines. J. Virol. Methods *193*, 639–646.

Ricagno, S., Egloff, M.P., Ulferts, R., Coutard, B., Nurizzo, D., Campanacci, V., Cambillau, C., Ziebuhr, J., and Canard, B. (2006). Crystal structure and mechanistic determinants of SARS coronavirus nonstructural protein 15 define an endoribonuclease family. Proc. Natl. Acad. Sci. USA *103*, 11892–11897.

Roberts, A., Deming, D., Paddock, C.D., Cheng, A., Yount, B., Vogel, L., Herman, B.D., Sheahan, T., Heise, M., Genrich, G.L., et al. (2007). A mouse-adapted SARS-coronavirus causes disease and mortality in BALB/c mice. PLoS Pathog. *3*, e5.

Roby, J.A., Pijlman, G.P., Wilusz, J., and Khromykh, A.A. (2014). Noncoding subgenomic flavivirus RNA: multiple functions in West Nile virus pathogenesis and modulation of host responses. Viruses *6*, 404–427.

Shapiro, J.S., Varble, A., Pham, A.M., and Tenoever, B.R. (2010). Noncanonical cytoplasmic processing of viral microRNAs. RNA *16*, 2068–2074.

Shi, J., Sun, J., Wang, B., Wu, M., Zhang, J., Duan, Z., Wang, H., Hu, N., and Hu, Y. (2014). Novel microRNA-like viral small regulatory RNAs arising during human hepatitis A virus infection. FASEB J. *28*, 4381–4393.

tenOever, B.R. (2013). RNA viruses and the host microRNA machinery. Nat. Rev. Microbiol. *11*, 169–180.

Torres, A.G., Fabani, M.M., Vigorito, E., and Gait, M.J. (2011). MicroRNA fate upon targeting with anti-miRNA oligonucleotides as revealed by an improved Northern-blot-based method for miRNA detection. RNA *17*, 933–943.

Tycowski, K.T., Guo, Y.E., Lee, N., Moss, W.N., Vallery, T.K., Xie, M., and Steitz, J.A. (2015). Viral noncoding RNAs: more surprises. Genes Dev. *29*, 567–584.

Varble, A., Chua, M.A., Perez, J.T., Manicassamy, B., García-Sastre, A., and tenOever, B.R. (2010). Engineered RNA viral synthesis of microRNAs. Proc. Natl. Acad. Sci. USA *107*, 11519–11524.

Weng, K.F., Hung, C.T., Hsieh, P.T., Li, M.L., Chen, G.W., Kung, Y.A., Huang, P.N., Kuo, R.L., Chen, L.L., Lin, J.Y., et al. (2014). A cytoplasmic RNA virus generates functional viral small RNAs and regulates viral IRES activity in mammalian cells. Nucleic Acids Res. *42*, 12789–12805.

Werneke, S.W., Schilte, C., Rohatgi, A., Monte, K.J., Michault, A., Arenzana-Seisdedos, F., Vanlandingham, D.L., Higgs, S., Fontanet, A., Albert, M.L., and Lenschow, D.J. (2011). ISG15 is critical in the control of Chikungunya virus infection independent of UbE1L mediated conjugation. PLoS Pathog. *7*, e1002322.

Zúñiga, S., Cruz, J.L., Sola, I., Mateos-Gómez, P.A., Palacio, L., and Enjuanes, L. (2010). Coronavirus nucleocapsid protein facilitates template switching and is required for efficient transcription. J. Virol. *84*, 2169–2175.